

DEVELOPMENT OF 'LICK AND STICK' PASSIVE WIRELESS
TEMPERATURE SENSOR FOR HARSH ENVIRONMENT

HASANUL KARIM

Department of Mechanical Engineering

APPROVED:

Yirong Lin, Ph.D., Chair

Norman Love Jr., Ph.D.

Tzu-Liang (Bill) Tseng, Ph.D.

Benjamin C. Flores, Ph.D.
Dean of the Graduate School

Copyright ©

by

Hasanul Karim

2013

Dedication

My mother Mosammat Begum Nurjahan, my father Ali Karim, my brother Nazmul Karim, & my wife Naznin Jahan Afrose

PREVIEW

PREVIEW

DEVELOPMENT OF 'LICK AND STICK' PASSIVE WIRELESS
TEMPERATURE SENSOR FOR HARSH ENVIRONMENT

by

HASANUL KARIM, Bachelor of Science in Mechanical Engineering

THESIS

Presented to the Faculty of the Graduate School of
The University of Texas at El Paso
in Partial Fulfillment
of the Requirements
for the Degree of
MASTER OF SCIENCE

Department of Mechanical Engineering
THE UNIVERSITY OF TEXAS AT EL PASO

December 2013

UMI Number: 1551228

All rights reserved

INFORMATION TO ALL USERS

The quality of this reproduction is dependent upon the quality of the copy submitted.

In the unlikely event that the author did not send a complete manuscript and there are missing pages, these will be noted. Also, if material had to be removed, a note will indicate the deletion.



UMI 1551228

Published by ProQuest LLC (2014). Copyright in the Dissertation held by the Author.

Microform Edition © ProQuest LLC.

All rights reserved. This work is protected against unauthorized copying under Title 17, United States Code



ProQuest LLC.
789 East Eisenhower Parkway
P.O. Box 1346
Ann Arbor, MI 48106 - 1346

Acknowledgements

First, I would like to thank the Department of Energy for supporting this project. I want to express my gratitude to my supervisor Dr. Yirong Lin for giving me this research project and for all his support, advice, and encouragement. I would like to thank my committee members, Dr. Normal Love and Dr. Bill Tseng for agreeing to be on the defense committee. I want to especially thank to Mr. Diego Delfin, Dr. Sarah Gaytan and Ms. Monica Cadena for their contributions, help and suggestions in this project. I would like to thank W. M. Keck Center in UTEP for providing the facility to fabricate the samples. I am thankful to Mr. Cesar Garcia and Mr. Jay H Barton and Mr. Jeff Peebles for their kind and sincere help in the testing part of the project. I would like to thank Dr. Evgeny Shafirovich and his students for their help in the fabrication process. I would like to thank all the members of Dr. Lin's research group for their co-operation, help and invaluable suggestions throughout this project. I would like to thank Mr. Mohammad Arif Ishtiaque Shuvo and Mr. Md. Rajib for being such good friends and making things easier for me.

Lastly, but not the least, I am grateful to my dear wife Naznin Jahan Afrose. I could not have completed my thesis without her unlimited support and patience.

Abstract

Wireless passive temperature sensors have been receiving increasing attention due to the ever-growing need of higher energy efficient and precise monitoring of temperatures in high temperature energy conversion systems such as gas turbines and coal-based power plants. Unfortunately, the harsh environment such as high temperature and corrosive atmosphere present in these systems has significantly limited the reliability and increased the cost of current solutions. Therefore, this research project presents the concept and design of a low cost, passive, and wireless temperature sensor that can withstand high temperature and harsh environment. The temperature sensor was designed following the principle of metamaterials by utilizing Closed Ring Resonators (CRR) in a dielectric matrix. The proposed wireless, passive temperature sensor behaves like an LC circuit, which has a temperature dependent resonance frequency. A full wave electromagnetic solver Ansys Ansoft HFSS was used to validate the model and to evaluate the effect of different geometry and combination of SRR structures on the resonance frequency and sensitivity of the proposed sensor. Two different fabrication methods – compression method using a die-punch assembly and 3D printing using binder-jetting techniques were used to fabricate the sensors. To simplify the sensor design, commercially available metal washers were used as CRR structures. Barium Titanate (BTO), and Alumina (Al_2O_3) were used as dielectric materials. Material characterization was done using Scanning Electron Microscopy (SEM) and X-ray Diffraction (XRD), and preliminary free space testing at room temperature using horn antennas and Gaussian beam antennas very promising results for using this novel sensing system for harsh environment application.

Table of Contents

Acknowledgements	v
Abstract	vi
Table of Contents	vii
List of Tables	viii
List of Figures	ix
Chapter 1: Introduction	1
1.1 Introduction to metamaterials	1
1.2 Application of Metamaterials	7
1.3 Metamaterials in sensing technology	9
1.4 Conclusion	11
Chapter 2: Literature Review	12
2.1 Metamaterials	12
2.2 Wireless temperature sensing	17
2.3 Conclusion	19
Chapter 3: Model and Simulation	20
3.1 Concept and model of the sensor	20
3.2 Different SRR structure and their response with varying parameters	21
3.3 Effects of the substrate thickness (d) on Resonance Parameters	24
3.4 Effects of the split gap (g) on Resonance Parameters	27
3.5 Effect of relative permittivity (ϵ_r) on the resonance frequency	29
3.6 Comparison of the Electrical sizes of the sensor model with different SRR structure.....	30
3.7 Conclusion.....	31
Chapter 4: Fabrication	32
4.1 Fabrication using conventional die-punch assembly	32
4.2 Fabrication using 3D printing	40
4.3 Conclusion	53
Chapter 5: Testing and Results.....	55
5.1 Experimental setup using waveguide and network analyzer and corresponding test results	55
5.2 Experimental setup for free space measurement using horn antenna and corresponding test results	57
5.3 Experimental setup for free space measurement using Gaussian Beam antenna and corresponding test results	61
5.4 Conclusion.....	66
Chapter 6: Conclusion	67
References	69
Curriculum Vita.....	76

List of Tables

Table 4.1: Waveguide specifications	34
Table 4.2: Summary of fabricated samples	35

PREVIEW

List of Figures

Figure 1.1: Directions of the Electric (E) and Magnetic (H) vector fields, wave vector (k) and the power flow density (S) vector in (a) Right Handed Medium and (b) Left Handed Medium.....	3
Figure 1.2: Light ray passing from medium 1 to medium 2. 1) incident ray, 2) Reflected ray, 3) refracted ray in a right handed medium and 4) refracted ray in a left handed medium	4
Figure 1.3: Different excitation techniques for SRR structure (a) only magnetic excitation (b) electric and magnetic excitation (c) only electric excitation and (d) no excitation. [9]	5
Figure 1.4: A square array of the first SRR structure proposed by Pendry et al. with lattice spacing a [10].	6
Figure 1.5: Some SRR structures studied in literature [12-15]	7
Figure 1.6: (A) 2D and (B) 3D paths that a light will follow theoretically through a cloaking device. [20]	8
Figure 1.7: (a) Schematic of the micrometer-sized metamaterial resonators sprayed on paper substrates with a predefined microstencil (b) Fabricated sample (c) Optical microscopy image of an as fabricated paper metamaterial sample	10
Figure 2.1: Photograph of an as built thermal cloak by Schittny et al. [83]	16
Figure 2.2: Schematic of wireless sensing of integrated resonator/antenna sensor developed by Cheng et al. [99]	18
Figure 3.1: (a) Proposed model of the temperature sensor (b) Equivalent circuit	21
Figure 3.2: Proposed sensor based on CRR structure modeled in Ansys Ansoft HFSS	22
Figure 3.3: Sensor model with different SRR structures: (a) EC-SRR (b) DSRR (c) BC-SRR (d) BC-CSRR (e) MSRR (f) DMSRR	22
Figure 3.4: An DMSRR model showing all the geometry parameters	23
Figure 3.5: Transmission spectrum, (a) CRR, (b) EC-SRR	24
Figure 3.6: Transmission spectrum, (a) DSRR (b) BC-SRR sensor structures.....	25
Figure 3.7: Transmission spectrum, (a) DMSRR (b) BC-CSRR sensor structures.	25
Figure 3.8: (a) Transmission spectra, MSRR structure (b) Effect of substrate thickness on resonance frequency for different SRR structured units.	26
Figure 3.9: Transmission spectra, (a) EC-SRR structure (b) DSRR structure	27
Figure 3.10: Transmission spectra, (a) BC-SRR structure (b) DMSRR structure	28
Figure 3.11: Transmission spectra, (a) BC-CSRR structure (b) MSRR structure	28
Figure 3.12: Effect of split gap on resonance frequency for different SRR structured units.....	29
Figure 3.13: (a) Transmission spectra, CRR structure (b) Effect of dielectric constant on resonance frequency for different SRR structured units.	30
Figure 4.1: Temperature and grain size influence in BaTiO ₃ properties [107]	33
Figure 4.2: (a) Schematic of sensor architecture, (b) die placed inside of the pressing machine, prior to compression.....	35
Figure 4.3: Sample 1, (a) top view, (b) 3D view	36
Figure 4.4: Sample 2, (a) top view, (b) 3D view	37
Figure 4.5: Sample 3, (a) top view, (b) 3D view	37
Figure 4.6: Sample 4, (a) top view, (b) 3D view	37
Figure 4.7: Sample 5, (a) top view, (b) 3D view	38
Figure 4.8: Sample 6, (a) top view, (b) 3D view	38
Figure 4.9: Sample 7, (a) top view, (b) 3D view	38

Figure 4.10: Sample 8, (a) top view, (b) 3D view	39
Figure 4.11: Samples polished for X band testing. Both (a) and (b) were fabricated under the same characteristics	39
Figure 4.12: Schematic of powder bed system [108]	40
Figure 4.13: As received BTO powder [108]	41
Figure 4.14: Different temperature profiles used for sintering fabricated parts [108]	42
Figure 4.15: Density vs sintering temperature for different binder saturations [108]	43
Figure 4.16: Set of magnified images (a) to (c) of sample fabricated with 60% binder saturation, layer thickness of 30 μm and sintered at 1200 $^{\circ}\text{C}$ for 4 hours [108]	44
Figure 4.17: Set of magnified images (a) to (c) of sample fabricated with 60% binder saturation, layer thickness of 30 μm and sintered at 1260 $^{\circ}\text{C}$ for four hours [108]	45
Figure 4.18: Set of magnified images (a) and (b) of sample fabricated with 60% binder saturation, layer thickness of 30 μm and sintered at 1330 $^{\circ}\text{C}$ for four hours [108]	46
Figure 4.19: Set of magnified images a) to c) of sample fabricated with 60% binder saturation, layer thickness of 30 μm and sintered at 1400 $^{\circ}\text{C}$ for four hours [108]	47
Figure 4.20: XRD analysis of as-received powder and sample sintered at 1260 $^{\circ}\text{C}$ for four hours [108]	48
Figure 4.21: Graph depicting shrinkage percentage in each direction vs sintering temperature [108]	49
Figure 4.22: CAD design of (a) Male part with extrusions (b) Female part with holes (c) Section view of the assembly	50
Figure 4.23: Fabricated male and female parts with BTO, sintered at 1260 $^{\circ}\text{C}$ for four hours	50
Figure 4.24: SEM image of raw alumina powder at different magnifications	51
Figure 4.25: Fabricated male and female parts using alumina (a) before sintering and (b) after sintering at 1680 $^{\circ}\text{C}$ for 4 hours	52
Figure 4.26: CAD design of curved sample of (a) 4.38 mm arc length and 4mm thickness (b) 20 mm arc length and 2.5 mm thickness	52
Figure 4.27: Fabricated curved samples (a) as built samples (b) small sample fitted inside the tube (c) large sample inside the tube	53
Figure 5.1: Experimental setup of measuring dielectric constant with a waveguide, a 3D printed BTO sample is placed in front of the setup	55
Figure 5.2: Dielectric constant of BTO samples fabricated by 3D printing and sintered at different temperatures as a function of frequency	56
Figure 5.3: Dielectric constant of an as built sample fabricated by compression method as a function of frequency	57
Figure 5.4: Free space measurement setup using horn antenna connected to a network analyzer	58
Figure 5.5: Transmission response measured from the scattered parameters for sample 3, 4, and 5 placed horizontally	59
Figure 5.6: Transmission response measured from the scattered parameters for sample 3, 4, and 5 placed vertically	60
Figure 5. 7: Free space testing setup with two Gaussian Beam antennas connected with a network analyzer (www.mwilab.com)	61
Figure 5.8: Transmission response from sample 1 (a) from 2-18 GHz (b) from 12-18 GHz	62
Figure 5.9: Transmission response from sample 2	63
Figure 5. 10: Transmission response from sample 3 (a) from 2-18 GHz (b) from 11-18 GHz	63
Figure 5.11: Transmission response from sample 4	64

Figure 5.12: Transmission response from sample 5.....	64
Figure 5.13: Transmission response from sample 6.....	65
Figure 5.14: Transmission response from sample 7.....	65
Figure 5.15: Transmission response from sample 8.....	66

PREVIEW

Chapter 1: Introduction

There is an increasing demand for the further development of sensing technologies in the energy conversion systems such as gas turbines, coal based power plants, and in automotive industries. Precise temperature sensing is one of the most critical parameters to safeguard better combustion, achieve higher efficiency and lower contaminant emissions to the environment. Since these combustion processes create a harsh environment of high temperature and corrosive conditions, it is imperative that the sensors are made to survive this environment and at the same time being reliable. Eventually, necessity of wireless sensors increased as the wired systems are found to be expensive, complicated, and they limit the operating temperatures. Previous efforts on the regime of wireless sensing include thermocouples, thermoelectric materials and fiber optics. However, most of the approach is limited due to either being complicated or expensive. Furthermore, low reliability has been identified as an issue while working on harsh environments due to the use of welded joints, energy storage devices, and semi-conductor materials in their arrangements [1-3]. Therefore, there is an ever-increasing interest in developing passive, wireless, low cost and reliable temperature sensors capable of working in the hostile environments present in energy conversion systems. This thesis is a proposal for a passive wireless temperature sensor for harsh environments inspired from the concept of metamaterials. This first chapter of the dissertation presents the background of the study, describes its significance, and provides an overview of the methodology used.

1.1 Introduction to metamaterials

Meta is a Greek word, which means “beyond”, hence the word “metamaterials” refers to materials that can display properties that are beyond the properties of natural materials. Usually the structure of these materials plays a significant role deciding its properties rather than the material properties of its components. When an electromagnetic wave passes through a material, the otherwise nonhomogeneous medium can be considered as a homogeneous medium if the

atoms of that material are very small compared to the wavelength of the incident electromagnetic wave. So, from the electromagnetic point of view, it is the wavelength λ that determines whether a collection of objects can be considered as a material or not. The block of objects might not be considered as a material by the conventional definition of materials but to the incident electromagnetic wave there is no difference and hence this can be considered as an artificial material or metamaterial [4]. Such homogeneous medium can be characterized by only two parameters: electric permittivity (ϵ) and magnetic permeability (μ). These two parameters are very important and determine the propagation characteristic of an electromagnetic wave through a medium, which can be shown by the dispersion equation. The dispersion relation for an isotropic medium is defined as:

$$k^2 - \frac{\omega^2}{c^2} n^2 = 0 \quad (1.1)$$

Where, k is the wavenumber, ω is the angular frequency, c is the velocity of light in vacuum and n is the refractive index of the substance, which is given by,

$$n = \sqrt{\mu_r \epsilon_r} \quad (1.2)$$

Where, μ_r is the relative permeability and ϵ_r is the relative permittivity of the medium. For most of the natural materials both relative permeability and permittivity are positive and hence n is also a positive number. As long as both μ_r and ϵ_r have the same sign, n is a real number and wave will propagate through the medium but, if one of them is negative then n becomes imaginary and there will be no transmission for a thick substance. Now, the significance of both negative ϵ_r and μ_r can be further investigated by examining Faraday's and Ampere's law. For a monochromatic plane wave that uses $e^{j\omega t}$ convention, Ampere's and Faraday's law are expressed in equation 1.3 and 1.4 respectively:

$$\vec{k} \times \vec{H} = -\omega \epsilon \vec{E} \quad (1.3)$$

$$\vec{k} \times \vec{E} = \omega \mu \vec{H} \quad (1.4)$$

Where, \vec{k} is the wave vector, \vec{H} and \vec{E} are magnetic and electric field intensity vectors respectively. When both ϵ and μ are positive, from equation (1.3) and (1.4) it can be seen that \vec{k} , \vec{H} and \vec{E} form a right-handed co-ordinate system whereas when they are both negative, the

vectors form a left-handed co-ordinate system. A comparison between left-handed and right-handed co-ordinates systems is shown in Figure 1.1. Veselago's proposal of an artificial medium that can have simultaneously negative values of permittivity (ϵ) and permeability (μ) in 1968 was actually the starting point of the research on

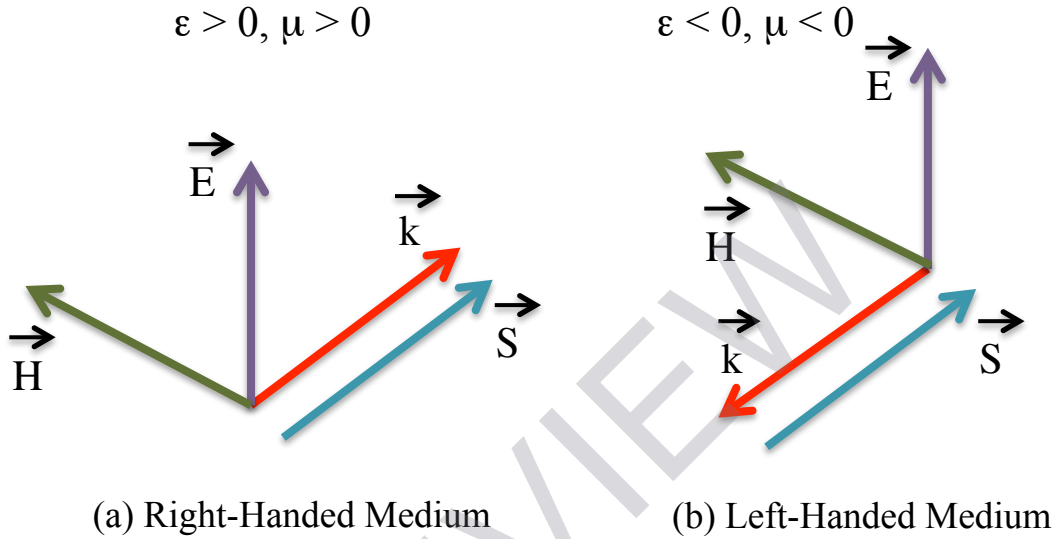


Figure 1.1: Directions of the Electric (E) and Magnetic (H) vector fields, wave vector (k) and the power flow density (S) vector in (a) Right Handed Medium and (b) Left Handed Medium

left-handed metamaterials [5]. It was expected that a left-handed medium would display some nonconventional behaviors such as backward propagation, reverse Doppler effect, reverse Vavilov-Cerenkov effect, and negative index of refraction [6]. The phenomenon of negative index of refraction can be explained with a modified Snell's law. When a ray of light passes from one medium to another medium the refraction of the light follows the general Snell's law (equation 1.5) if both media are right handed. As shown in Figure 1.2, the incident light ray is reflected along path 2 and refracted through path 3. However, if one of the media is left handed then a more accurate form of the Snell's law is used (equation 1.6). In that case, the refracted light goes along path 4.

$$\frac{\sin \theta}{\sin \phi} = \frac{n_2}{n_1} = \sqrt{\frac{\mu_2 \epsilon_2}{\mu_1 \epsilon_1}} \quad (1.5)$$

$$\frac{\sin \theta}{\sin \phi} = \frac{n_2}{n_1} = \frac{p_2}{p_1} \sqrt{\frac{\mu_2 \epsilon_2}{\mu_1 \epsilon_1}} \quad (1.6)$$

Where p_1 and p_2 are the rightness of the first and second medium respectively. p is +1 for a right handed medium and it is -1 for a left handed medium.

Negative values of permeability and permittivity can be obtained by combining special resonator structures with appropriate excitation techniques. There are three types of excitations that can be used for metamaterial resonator structures. They are: magnetic excitation, electric excitation and both magnetic and electrical excitation [6-8]. The choice of the excitation depends on the desired application. If ENG regions are required, the structure has to be excited electrically and it has to be excited

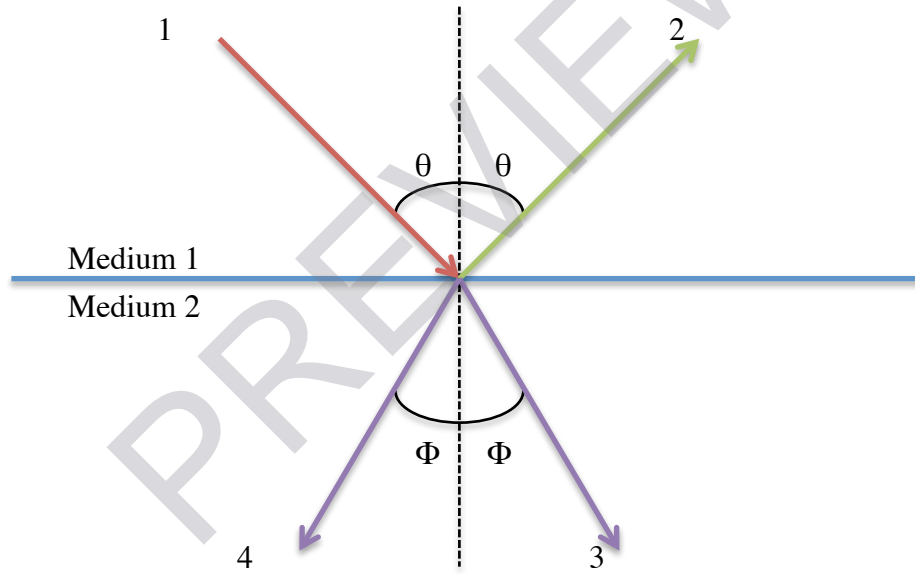


Figure 1.2: Light ray passing from medium 1 to medium 2. 1) incident ray, 2) Reflected ray, 3) refracted ray in a right handed medium and 4) refracted ray in a left handed medium

magnetically in order to obtain MNG regions [8]. Figure 1.3 summarizes the excitation techniques for a SRR structure. In figures 1.3(a) and 1.3(b), the magnetic field is perpendicular to the SRR plane. Hence, according to the Faraday's law of induction it can excite the magnetic resonances of the SRR. On the other hand when the magnetic field is parallel to the SRR plane it cannot excite a magnetic resonance. In figures 1.3(b) and 1.3(c), the electric field is

perpendicular to the gap of the rings. This configuration can excite the electrical resonances of the structure. Hence, the structure in figure 1.3(b) is excited both electrically and magnetically and the structure at 1.3(d) is not excited at all from the sense of an LC circuit.

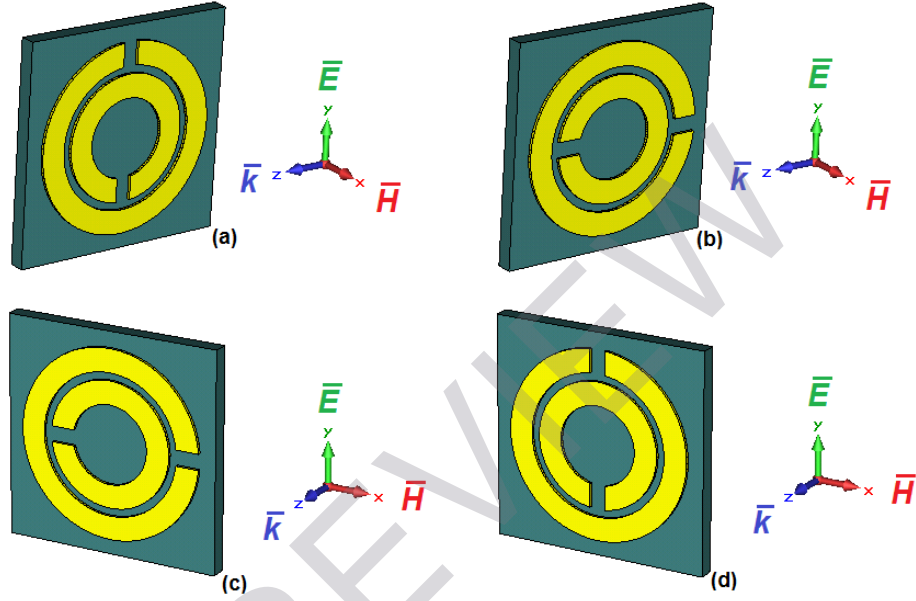


Figure 1.3: Different excitation techniques for SRR structure (a) only magnetic excitation (b) electric and magnetic excitation (c) only electric excitation and (d) no excitation. [9]

Prior to the development of metamaterials, materials with single negative index were found in nature, which were either Epsilon Negative media (ENG) or Mu Negative media (MNG). The concept of a Double Negative media (DNG) or Left Handed Media (LHM) was exciting, but it was not realized in reality until in 1999 when J.B. Pendry et al. [10] proposed the use of periodical arrays of SRRs (Split Ring Resonators) and thin-wires together where the negative values of effective permeability are obtained from the SRR structure and the negative values of permittivity are obtained from the thin wire array. It has been demonstrated that metamaterials need to appear as an effectively homogeneous media, which means that their lattice constants have to be smaller than the wavelength of the incident radiation [11].